Dyadic Green's Function for Electric Dipole Excitation of a Perfect Electromagnetic Conductor Sphere

Maryam Hesari-Shermeh, Mehri Ziaee-Bideskan, Mohsen Ghaffari-Miab, *Member, IEEE*, Bijan Abbasi-Arand, *Member, IEEE*, and Keyvan Forooraghi, *Member, IEEE*

***Abstract*—In this paper, we investigate the dyadic Green's function (DGF) of a perfect electromagnetic conductor sphere (PEMCS) due to electric dipoles, theoretically by employing the scattering superposition principle (SSP) and the Ohm-Rayleigh method. Then the derived DGF is used to calculate the scattered field of a PEMCS due to an arbitrarily oriented infinitesimal electric dipole and also plane wave illumination. Numerical results are compared with those obtained by FEKO commercial software to demonstrate the efficiency and accuracy of the proposed method. The results are in excellent agreement.**

***Index Terms*—Dyadic Green's functions (DGF), Ohm-Rayleigh method, Perfect electromagnetic conductor (PEMC), scattering superposition principle (SSP).**

I. Introduction

SCATTERING of electromagnetic waves from different objects is an important problem in electromagnetics which has been solved with numerous methods in past decades [1]– [5]. Among them, the concept of dyadic Green's function (DGF) has been employed widely as an attractive and powerful tool to formulate different electromagnetic boundary value problems.DGF of classical problems, including an infinite PEC and dielectric cylinders and spheres, different kinds of waveguides and cavities, have been derived earlier [5]. Moreover, stratified multilayered media [6]– [8], a dielectric elliptical cylinder [9] a dielectric spheroid [10] and a conical cavity with impedance spherical cap [11] are reported in literature. Also, the method is applied to more complex structures involving inhomogeneous, moving, bi-anisotropic and chiral media [12]– [15].

Recently a new class of boundary condition is introduced by *Lindell* and *Sihvola*, which is a nonreciprocal extension of both PEC and PMC, namely perfect electromagnetic conductor (PEMC) [16]– [17]. This idealized medium is characterized by a real scalar parameter, M, indicating the PEMC admittance (Ω^{-1}). This parameter makes a linear relation between total electric and magnetic fields which has to vanish in a PEMC medium, as

$$\overline{H} + M\overline{E} = 0, \qquad \overline{D} - M\overline{B} = 0. \tag{1}$$

This work was supported by Tarbiat Modares University under Grant IG-39703. (Corresponding author: Mohsen Ghaffari-Miab.)

The authors are with the Department of Electrical and Computer Engineering, Tarbiat Modares University, Tehran, 1411713-116 Iran, email:(m.hesari@modares.ac.ir, mehri.ziaee@modares.ac.ir, mghaffari@modares.ac.ir, Abbasi@modares.ac.ir, keyvan_f@modares.ac.ir)

It can be proved that for real values of M, the complex Poynting vector is imaginary and therefore the electromagnetic energy cannot be conveyed into a PEMC medium [18] and consequently, PEMC boundary will be referred as an ideal boundary with following boundary conditions

$$\hat{n} \times \left(\overline{H} + M\overline{E}\right) = 0, \qquad \hat{n}.\left(\overline{D} - M\overline{B}\right) = 0. \tag{2}$$

Since 2005, when the PEMC boundary condition introduced, it has attracted lots of attention. In [19]– [24], the electromagnetic scattering from different structures with PEMC boundary has been investigated.

According to (2), this boundary acts as a perfect reflector of electromagnetic waves like PEC and PMC except the fact that it creates non-reciprocal reflection. Reduction of a co-polarized radar cross section or designing a twist polarizer can be referred as the application of this unique property which clears the importance of PEMC [25]– [26]. In order to use this boundary in antenna and microwave applications, first, its practical realization must be investigated. Realization of this boundary has been studied in several papers [17]– [18], [27]. Recently, two different structures, due to their Faraday rotation effect, have been suggested for realizing such a boundary. In [28] a grounded ferrite slab which practically acts as a PEMC boundary has been proposed. Moreover, it was found that graphene is a good candidate for supporting giant Faraday rotation effect [29]. This discovery led to the introduction of PEMC boundaries based on graphene [30].

Among all the research work carried out on the PEMC boundary-value problems, [31]– [34] paid attention to the problem of DGF in such medium. In [35], plane wave scattering from a PEMCS has been investigated but to the best of our knowledge, DGF of this structure has not been studied yet. Hence, in this paper the DGF of a PEMCS generated by electric dipoles is extracted theoretically by employing the scattering superposition principle (SSP) and the Ohm-Rayleigh method. On the other hand, we extend the theory of DGF for an electric dipole in the vicinity of a PEC sphere (PECS) given in [5] to a more general case of PEMCS. Also, numerical results involving scattered field from a PEMCS by an arbitrarily oriented infinitesimal electric dipole and plane wave illumination are presented. Besides, the effect of different PEMC parameter values (M) on the extracted fields is reported.

The rest of the paper is organized as follows: In Section II fundamental formulas of the problem and rigorous formulation of the scattered DGF for the PEMCS is presented. Section III

This article has been accepted for publication in a future issue of this journal, but has not been fully edited. Content may change prior to final publication. Citation information: DOI 10.1109/TAP.2020.3037726, IEEE Transactions on Antennas and Propagation

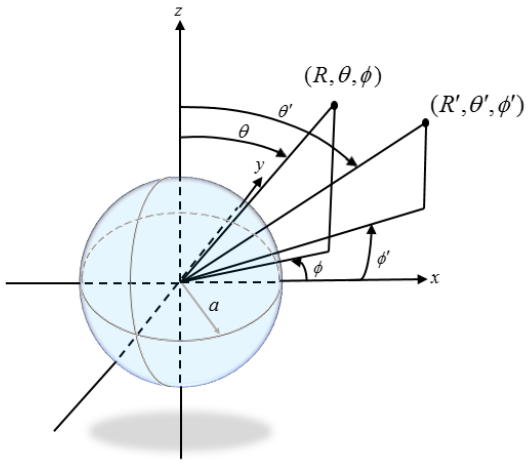

Fig. 1. An electric source located at (R', θ', φ') in the presence of a PEMCS.

is devoted to the numerical results of scattered field pattern from a PEMCS by using the derived DGF. Finally, Section IV concludes the work.

II. Formulation of the Boundary-Value Problem

In this section the closed-form DGF of the problem under study is derived. It should be noted that the time dependence is assumed to be $e^{-j\omega t}$ in our work.

A. Boundary condition

As we know, the boundary conditions satisfied at the surface of PEC and PMC are

$$\begin{array}{ll} \hat{n}\times\overline{E}=0\ , & (PEC) \\ \hat{n}\times\overline{H}=0\ . & (PMC) \end{array} \tag{3}$$

Since PEMC is an extension of both PEC and PMC, the linear combination of electromagnetic fields at the surface of a PEMC boundary is required to vanish, hence the desired boundary condition is [9]

$$\hat{n}\times\left(\overline{H}+M\overline{E}\right)=0, \tag{4}$$

where $\widehat{n}$ and M are the unit vector normal to the PEMC and PEMC admittance parameter, respectively.

Since M is an admittance like parameter (Ω^{-1}), we can consider PEMC boundary as a special kind of surface impedance boundary [36]– [37]. Hence, one can rewrite boundary condition of (4) as follows

$$\hat{n}\times\overline{E}=\overline{\overline{Z}}_s.\overline{H}, \tag{5}$$

where $\overline{\overline{Z}}_s$ is the surface impedance dyadic. Comparing the above equation with (4) reveals that the surface impedance for a PEMC boundary has the following form

$$\overline{\overline{Z}}_s=-\frac{1}{M}\hat{n}\times\overline{\overline{I}}, \tag{6}$$

where $\overline{\overline{I}}$ is idem factor. This relation, confirms the fact that PEMC is a nonreciprocal boundary when M has a finite nonzero value, which is the most noticeable property of the PEMC. Existence of cross-polarized scattered field is the result of this non-reciprocity which is not the case for PEC or PMC.

This is the key property which may have practical applications in transforming polarization including co-polarized RCS reduction. In special case, when $M = 0$ PEMC boundary condition acts as a PMC boundary while at $M \to \infty$ it reduces to a PEC boundary.

In order to state dyadic PEMC boundary condition, we should transform (4) into its dyadic form by considering three sets of fields produced by three orthogonal distinct current sources [5]. Under this condition, the notations $\overline{\overline{G}}_e$ and $\overline{\overline{G}}_m$ will be used to define electric and magnetic DGFs, as $\overline{\overline{E}}=\overline{\overline{G}}_e$ and $j\omega\mu_0\overline{\overline{H}}=\overline{\overline{G}}_m$ respectively. The electric $(\overline{\overline{G}}_e)$ and magnetic $(\overline{\overline{G}}_m)$ DGFs are the solutions of following dyadic differential eqtions

$$\nabla\times\nabla\times\overline{\overline{G}}_e(\overline{R},\overline{R'})-k^2\overline{\overline{G}}_e(\overline{R},\overline{R'})=\overline{\overline{I}}\delta(\overline{R},\overline{R'}), \tag{7}$$

$$\nabla\times\nabla\times\overline{\overline{G}}_m(\overline{R},\overline{R'})-k^2\overline{\overline{G}}_m(\overline{R},\overline{R'})=\nabla\times\left[\overline{\overline{I}}\delta(\overline{R},\overline{R'})\right], \tag{8}$$

in which, δ and k denote Dirac delta and wavenumber of the meduim, respectively. As a result, dyadic PEMC boundary condition at the sphere surface $R = a$, is stated as

$$\hat{R}\times(\overline{\overline{G}}_m+j\omega\mu_0M\overline{\overline{G}}_e)=0, \tag{9}$$

where $\widehat{R}$ is the unit vector normal to the surface of the PEMCS. By substituting $\overline{\overline{G}}_m=\nabla\times\overline{\overline{G}}_e$, one can express (9) in terms of only the electric DGF at $R = a$ as

$$\hat{R}\times(\nabla\times\overline{\overline{G}}_e+j\omega\mu_0M\overline{\overline{G}}_e)=0. \tag{10}$$

B. Eigen function expansion of the free space DGF

The geometry of the problem is shown in Fig. 1, in which the current source is located in position $\overline{R'}=(R',\theta',\varphi')$ while the observation point is at $\overline{R}=(R,\theta,\varphi)$. To find the DGF for the PEMCS, first the free space DGF calculated in [5] is presented and then by using the method of SSP, the DGF of the PEMCS is determined.

The eigen-function expansion of the free-space electric DGF, $\overline{\overline{G}}_{e0}$, in spherical coordinates satisfies (7) and can be drived by means of Ohm-Rayleigh method. The corresponding expression for $\overline{\overline{G}}_{e0}$ is then given by [5]

$$\overline{\overline{G}}_{e0}(\overline{R},\overline{R'})=-\frac{1}{k^2}\hat{R}\hat{R}\delta(\overline{R}-\overline{R'})$$
$$+\frac{jk}{4\pi}\sum_{m,n}C_{mn}\begin{cases}\left[\begin{array}{l}\overline{M}^{(1)}_{\substack{e\\o}mn}(k)\,\overline{M}'_{\substack{e\\o}mn}(k)+\\ \overline{N}^{(1)}_{\substack{o\\e}mn}(k)\,\overline{N}'_{\substack{o\\e}mn}(k)\end{array}\right] & R>R' \\ \left[\begin{array}{l}\overline{M}_{\substack{e\\o}mn}(k)\,\overline{M}'^{(1)}_{\substack{e\\o}mn}(k)+\\ \overline{N}_{\substack{o\\e}mn}(k)\,\overline{N}'^{(1)}_{\substack{o\\e}mn}(k)\end{array}\right] & R<R'\end{cases} \tag{11}$$

It should be noted that each term in the above summation has been formed as the sum of even and odd wave-functions, for example $\overline{M}^{(1)}_{\substack{e\\o}}\overline{M}'_{\substack{e\\o}}=\overline{M}^{(1)}_{e}\overline{M'}_{e}+\overline{M}^{(1)}_{o}\overline{M'}_{o}$. In which

This article has been accepted for publication in a future issue of this journal, but has not been fully edited. Content may change prior to final publication. Citation information: DOI 10.1109/TAP.2020.3037726, IEEE Transactions on Antennas and Propagation

$$\overline{M}_{\substack{e\\o}mn}(k) = \nabla \times \left(\overline{\psi}_{\substack{e\\o}mn}\overline{R}\right), \tag{12}$$

$$\overline{N}_{\substack{e\\o}mn}(k) = \frac{1}{k}\nabla \times \nabla \times \left(\overline{\psi}_{\substack{e\\o}mn}\overline{R}\right), \tag{13}$$

$$\overline{\psi}_{\substack{e\\o}mn}(k) = j_n(kR)\,P_n^m(\cos\theta)\ \begin{matrix}\cos\\ \sin\end{matrix}\ m\varphi, \tag{14}$$

where $j_n(x)$and $P_n^m(cos\theta)$ denote spherical Bessel function of order n and associated Legendre functions of order (n, m), respectively. Also

$$C_{mn} = (2-\delta_0)\frac{2n+1}{n(n+1)}\frac{(n-m)!}{(n+m)!}, \tag{15}$$

where δ_0 is the Kronecker delta function defined as $\delta_0 = \begin{cases} 1, & m=0 \\ 0, & m\neq 0 \end{cases}$, $\overline{\psi}_{\substack{e\\o}mn}$ is the solution of scalar wave equation in spherical coordinates, $\overline{M}_{\substack{e\\o}mn}(k)$ and $\overline{N}_{\substack{o\\e}mn}(k)$, are spherical vector wave-functions and describe the electric field of TE_{mn} and TM_{mn} modes, respectively. The superscript (1) is defined with respect to the spherical Hankel function of the first kind and the primed functions are defined with respect to (R', θ', φ') [5].

C. Deriving DGF of a PEMCS

By knowing the free space electric DGF and applying the method of SSP, we can calculate the DGF for a PEMCS as

$$\overline{\overline{G}}_e(\overline{R},\overline{R'}) = \overline{\overline{G}}_{e0}(\overline{R},\overline{R'}) + \overline{\overline{G}}_{es}(\overline{R},\overline{R'}), \tag{16}$$

where $\overline{\overline{G}}_{es}$ represents the scattered term. Considering $\overline{\overline{G}}_{e0}$, the $\overline{\overline{G}}_{es}$ can be written as

$$\overline{\overline{G}}_{es}(\overline{R},\overline{R'}) = \frac{jk}{4\pi}\sum_{m,n} C_{mn}\left\{\begin{bmatrix} A^{TE}\overline{M}^{(1)}(k)+ \\ B^{TE}\overline{N}^{(1)}(k)\end{bmatrix}\overline{M'}^{(1)}(k) + \begin{bmatrix} A^{TM}\overline{M}^{(1)}(k)+ \\ B^{TM}\overline{N}^{(1)}(k)\end{bmatrix}\overline{N'}^{(1)}(k)\right\}, \tag{17}$$

In order to simplify the writing, we dropped the subscript $\substack{e\\o}mn$ in vector wave functions.

$\overline{M}^{(1)}$ and $\overline{N}^{(1)}$ are the field function and are chosen due to the fact that scattered field must consist of outgoing waves. The excitation functions, $\overline{M'}^{(1)}$ and $\overline{N'}^{(1)}$, are dictated by the boundary condition at $R = a$ which can be satisfied only if the excitation functions are the same as that of $\overline{\overline{G}}_{e0}$ for $R < R'$. As it is seen, in order to satisfy the boundary condition at the surface of the PEMCS, the field function with coefficient B^{TE} (A^{TM}) has been added to the field function with coefficient A^{TE} (B^{TM}). This means that, for a linearly polarized incident field, for example TE, the scattered field from a PEMC boundary has a cross-polarized term, TM, as well as co-polarized component in general case. For the PMC and PEC special cases ($M = 0$ and $M \to \infty$, respectively) the cross-polarized component vanishes. In order to determine the unknown coefficients A^{TE}, B^{TE}, A^{TM} and B^{TM}, PEMC boundary condition at the surface of the sphere must be applied.

The tangential field components have to satisfy (10) at the sphere surface and is written as (18).

After some mathematical manipulations, a system of four linear equations is obtained which can be grouped into two independent system of equations as follows

$$\begin{aligned}[\mathrm{A}_1]\,[\mathrm{B}_1] &= [C_1]\,,\\ [\mathrm{A}_2]\,[\mathrm{B}_2] &= [C_2]\,.\end{aligned} \tag{19}$$

Where, the square matrices $[A_1]$ and $[A_2]$ as well as the column matrices $[B_1]$, $[B_2]$, $[C_1]$ and $[C_2]$ are defined as

$$\begin{aligned}
[\mathrm{A}_1] &= \begin{bmatrix} \frac{1}{a}Dh_a & \frac{q}{ka}Dh_a \\ qh_n^{(1)}(ka) & kh_n^{(1)}(ka)\end{bmatrix},\\
[\mathrm{B}_1] &= \begin{bmatrix} \mathrm{A}_n^{TE} & \mathrm{B}_n^{TE}\end{bmatrix}^{\mathrm{T}},\\
[C_1] &= \begin{bmatrix} -\frac{1}{a}Dj_a & -qj_n(ka)\end{bmatrix}^{\mathrm{T}},\\
[\mathrm{A}_2] &= \begin{bmatrix} \frac{1}{a}Dh_a & \frac{1}{ka}Dh_a \\ qh_n^{(1)}(ka) & kh_n^{(1)}(ka)\end{bmatrix},\\
[\mathrm{B}_2] &= \begin{bmatrix} \mathrm{A}_n^{TM} & \mathrm{B}_n^{TM}\end{bmatrix}^{\mathrm{T}},\\
[C_2] &= \begin{bmatrix} -q\frac{1}{ka}Dj_a & -kj_n(ka)\end{bmatrix}^{\mathrm{T}},
\end{aligned} \tag{20}$$

in which Dh_a, Dj_a and q are

$$\begin{aligned}
Dh_a &= \frac{\partial}{\partial R}\left[Rh_n^{(1)}(kR)\right]\Big|_{R=a},\\
Dj_a &= \frac{\partial}{\partial R}\left[Rj_n(kR)\right]|_{R=a},\\
q &= j\omega\mu_0 M.
\end{aligned} \tag{21}$$

Hence, the unknown scattering coefficients are determined as

$$A^{TE} = -\frac{j_n(ka)}{h_n^{(1)}(ka)} - \frac{\left(h_n^{(1)}(ka)Dj_a - j_n(ka)Dh_a\right)}{h_n^{(1)}(ka)Dh_a\left[1-\frac{q^2}{k^2}\right]}, \tag{22}$$

$$B^{TE} = \frac{q\left(h_n^{(1)}(ka)Dj_a - j_n(ka)Dh_a\right)}{h_n^{(1)}(ka)Dh_a\left[k-\frac{q^2}{k}\right]}, \tag{23}$$

$$A^{TM} = B^{TE}, \tag{24}$$

$$B^{TM} = -\frac{Dj_a}{Dh_a} - \frac{\left(j_n(ka)Dh_a - h_n^{(1)}(ka)Dj_a\right)}{h_n^{(1)}(ka)Dh_a\left[1-\frac{q^2}{k^2}\right]}. \tag{25}$$

A^{TE} and B^{TM} are the co-polarized coefficients, whereas the cross-polarized coefficients are defined by B^{TE} and A^{TM} for TE and TM polarization, respectively.

By replacing M with $M \to \infty$ and $M = 0$ in above equations, the scattering coefficients for the two special cases, PEC and PMC will be determined easily. Hence, for the PEC case,

This article has been accepted for publication in a future issue of this journal, but has not been fully edited. Content may change prior to final publication. Citation information: DOI 10.1109/TAP.2020.3037726, IEEE Transactions on Antennas and Propagation

$$\hat{R}\times\sum_{m,n}\left[\begin{array}{l}\left[k\left(\overline{N}(k)+A^{TE}\overline{N}^{(1)}(k)+B^{TE}\overline{M}^{(1)}(k)\right)+j\omega\mu_0 M\left(\overline{M}(k)+A^{TE}\overline{M}^{(1)}(k)+B^{TE}\overline{N}^{(1)}(k)\right)\right]\overline{M'}^{(1)}(k)+\\ \left[k\left(\overline{M}(k)+A^{TM}\overline{N}^{(1)}(k)+B^{TM}\overline{M}^{(1)}(k)\right)+j\omega\mu_0 M\left(\overline{N}(k)+A^{TM}\overline{M}^{(1)}(k)+B^{TM}\overline{N}^{(1)}(k)\right)\right]\overline{N'}^{(1)}(k)\end{array}\right]=0. \tag{18}$$

scattering co-polarized coefficients are $A^{TE}=-\dfrac{j_n(ka)}{h_n^{(1)}(ka)}$, $B^{TM}=-\dfrac{Dj_a}{Dh_a}$ and cross-polarizated terms vanishes due to PEC boundary conditions, which are the same as scattering coefficients from a PEC sphere given by [5]. As a result of duality theorem, for the PMC case, the co-polarized scattering coefficients are dual to PEC and cross-polarized scattering coefficients are zero.

Magnetic DGF is simply obtained as

$$\overline{\overline{G}}_m=\nabla\times\overline{\overline{G}}_e \tag{26}$$

Knowing the scattered coefficients and hence electric and magnetic DGF, we can determine the electromagnetic fields. As discussed in [5], these fields will be obtained by means of the following equations

$$\overline{E}(\overline{R})=j\omega\mu_0\int_{v'}\overline{\overline{G}}_e(\overline{R},\overline{R'}).\overline{J}(\overline{R'})dv'. \tag{27}$$

$$\overline{H}(\overline{R})=j\omega\mu_0\int_{v'}\overline{\overline{G}}_m(\overline{R},\overline{R'}).\overline{J}(\overline{R'})dv'. \tag{28}$$

The domain of the integration is through the entire volume of the source.

In the following section we calculate the scattered field excited by a horizontal and vertical electric dipole (HED and VED) in the vicinity of the PEMCS as well as a plane wave scattering as special cases, but this method is not restricted to these kind of electric sources and any arbitrary source can be chosen.

III. Numerical results and discussion

In this section we calculate scattered fields from the PEMCS with radius equal to $a=\lambda/3$ excited by three different current distributions. We first analyze a HED in vicinity of the PEMCS and then the case of a VED with dipole position at $b=2a$. Finally plane wave scattering from the PEMCS will be discussed. In all three cases we have plotted the results at $\phi=\pi/3$ and compared them with those of full wave simulator, FEKO, which are in excellent agreement.

A. HED

For an infinitesimal HED with current moment c pointed in the x-direction and located at $R'=b,\theta'=0,\phi'=0$, we let

$$\overline{J}(\overline{R'})=c\frac{\delta(R'-b)\delta(\theta'-0)\delta(\varphi'-0)}{b^2\sin\theta'}\hat{x}. \tag{29}$$

Using the expression for $\overline{\overline{G}}_{es}$ given by (17)–(25), the scattered field produced by this HED is obtained by substituting $\overline{\overline{G}}_{es}$ and (29) in (27) as follows

$$\overline{E}_s(\overline{R})=\frac{k\omega\mu_0 c}{4\pi}\sum_{n=1}^{\infty}\frac{2n+1}{n(n+1)}\left\{\begin{array}{l}\left(B^{TE}h_n^{(1)}(kb)+\dfrac{1}{kb}(kbh_n^{(1)}(kb))'B^{TM}\right)\overline{N}_{e1n}^{(1)}(k)+\\ \left(A^{TE}h_n^{(1)}(kb)+\dfrac{1}{kb}(kbh_n^{(1)}(kb))'A^{TM}\right)\overline{M}_{o1n}^{(1)}(k)\end{array}\right\} \tag{30}$$

Since $\varphi'=0,\theta'=0$, the HED is directed along $\widehat{\theta}$, and only $\overline{M}_{o1n}$ and $\overline{N}_{e1n}$ are nonzero. Therefore TE_{1n} and TM_{1n} are the only excited modes. In order to plot these components of the scattered field a dimensionless parameter α is defined as

$$\alpha=\tan^{-1}(M\eta_0). \tag{31}$$

With this definition, the limiting case of PEC surface ($M\to\infty$) is equal to $\alpha=90^\circ$.

The scattered field in $x-z$ plane for the PEMC parameter $\alpha=30^\circ$ is obtained and plotted in Fig. 2.

We shall now derive scattered electric far-field. For this purpose, we should use an asymptotic form of spherical Hankel function for $kR>>1$ as

$$\begin{aligned}h_n^{(1)}(kR)&\simeq(-j)^{n+1}\frac{e^{jkR}}{kR},\\ \frac{\left[kRh_n^{(1)}(kR)\right]'}{kR}&\simeq(-j)^n\frac{e^{jkR}}{kR}.\end{aligned} \tag{32}$$

By substituting (32) in (30), scattered electric far-field will be derived as follows

$$E_{s,R}\simeq 0, \tag{33}$$

$$E_{s,\theta}=\omega\mu_0 c\frac{e^{jkR}}{4\pi R}\sum_{n=1}^{\infty}\frac{2n+1}{n(n+1)}(-j)^n\left\{\begin{array}{l}\left(B^{TE}h_n^{(1)}(kb)+\dfrac{B^{TM}}{kb}(kbh_n^{(1)}(kb))'\right)N_\theta-\\ j\left(A^{TE}h_n^{(1)}(kb)+\dfrac{A^{TM}}{kb}(kbh_n^{(1)}(kb))'\right)M_\theta\end{array}\right\}, \tag{34}$$

$$E_{s,\varphi}=\omega\mu_0 c\frac{e^{jkR}}{4\pi R}\sum_{n=1}^{\infty}\frac{2n+1}{n(n+1)}(-j)^n\left\{\begin{array}{l}\left(B^{TE}h_n^{(1)}(kb)+\dfrac{B^{TM}}{kb}(kbh_n^{(1)}(kb))'\right)N_\varphi+\\ j\left(A^{TE}h_n^{(1)}(kb)+\dfrac{A^{TM}}{kb}(kbh_n^{(1)}(kb))'\right)M_\varphi\end{array}\right\}. \tag{35}$$

This article has been accepted for publication in a future issue of this journal, but has not been fully edited. Content may change prior to final publication. Citation information: DOI 10.1109/TAP.2020.3037726, IEEE Transactions on Antennas and Propagation

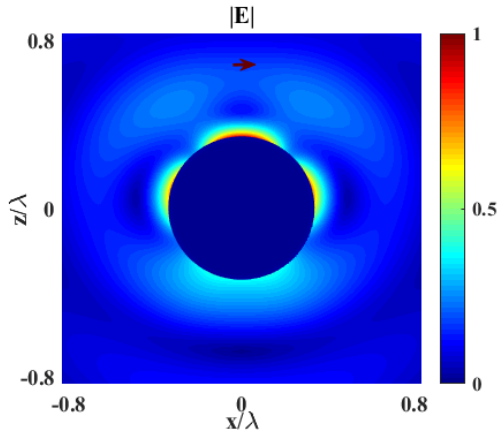

Fig. 2. The normalized absolute value of scattered field in $x-z$ plane due to a HED directed to the x axis for $\alpha = 30°$.

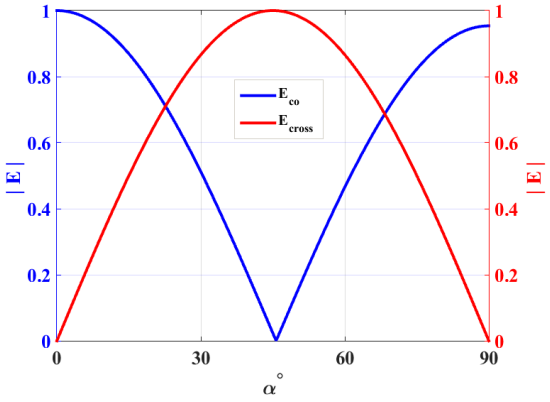

Fig. 3. Co- and cross-polarized terms of normalized absolute value of scattered electric far-field versus $\alpha°$ at $\theta = 0°$ for HED.

where

$$\begin{cases} N_\theta = \dfrac{\partial}{\partial\theta} P_n^1(\cos\theta)\cos\varphi \\ M_\theta = \dfrac{1}{\sin\theta} P_n^1(\cos\theta)\cos\varphi \end{cases}, \tag{36}$$

$$\begin{cases} N_\varphi = \dfrac{1}{\sin\theta} P_n^1(\cos\theta)\, sin\varphi \\ M_\varphi = \dfrac{\partial}{\partial\theta} P_n^1(\cos\theta)\sin\varphi \end{cases}.$$

Finally,

$$\left|\overline{E}_s\left(\overline{R}\right)\right| = \sqrt{|E_{s,\theta}|^2 + |E_{s,\varphi}|^2}. \tag{37}$$

Co- and cross-polarized scattered electric far-field as a function of α is plotted in Fig. 3.

According to Fig. 3, for some values of M (α), co-polarized component is dominant, while for the others, cross-polarized component is dominant. For $\alpha = 0°$ and $\alpha = 90°$ the cross-polarized term is vanished as expected. Depending on the application, the proper value for M should be chosen. Regarding our numerical experience for the summation in (34) and (35) to be converged, only first few terms are sufficient.

To investigate the convergence behaviour in detail, the scattered field as a function of n for different values of a/λ at $\alpha = 60°$ is plotted in Fig. 4. As can be seen from the figure, for $a/\lambda = 0.5$, 1, 1.5, and 2, the results are converged after $n = 6$, 9, 12, and 15, respectively, with relative error of less than 0.02% . The converged results obtained for $n = 20$ are assumed as the reference for calculating the relative error. As it is expected, increasing the radius results in a slower convergence.

Furthermore, different values of a/λ is equivalent to different frequencies for a fixed sphere radius a. As long as a/λ is constant, the scattered fields are independent of frequency.

Next, the effect of different values of PEMC parameter (M or α) on the scattered field is investigated and plotted in Fig. 5 and 6. As it can be seen from Fig. 5, by increasing the PEMC parameter, the pattern shifts toward the limiting case of PEC ($M \to \infty$ or $\alpha = 90°$). On the other hand, according to Fig. 6, decreasing M causes a shift toward to the other limiting case PMC ($M = 0$ or $\alpha = 0°$).

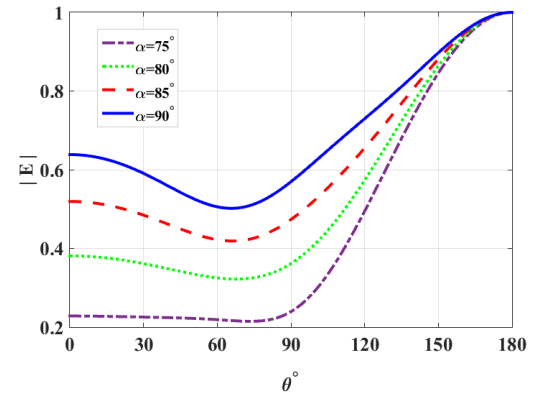

Fig. 5. Effect of PEMC parameter on the normalized absolute value of scattered electric far-field pattern; Increasing α toward 90°.

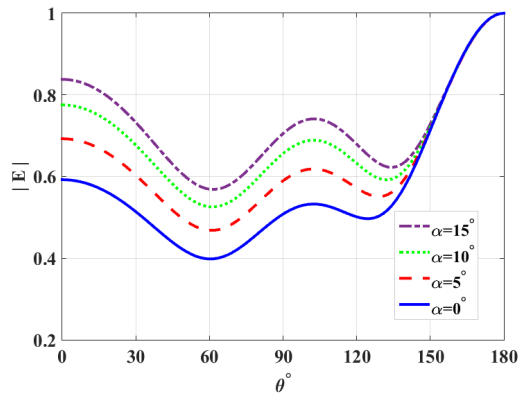

Fig. 6. Effect of PEMC parameter on the normalized absolute value of scattered electric far-field pattern; decreasing α toward 0°.

The above mentioned method for finding the scattered field for any arbitrary current distribution is very time effective with high accuracy and can be used as a benchmark for existing full-wave software. Moreover, there is no constraint on the sphere radius and the scattered field from any arbitrary radius can be computed while in commercial software we may run out of memory. Even with the use of parallel processing

This article has been accepted for publication in a future issue of this journal, but has not been fully edited. Content may change prior to final publication. Citation information: DOI 10.1109/TAP.2020.3037726, IEEE Transactions on Antennas and Propagation

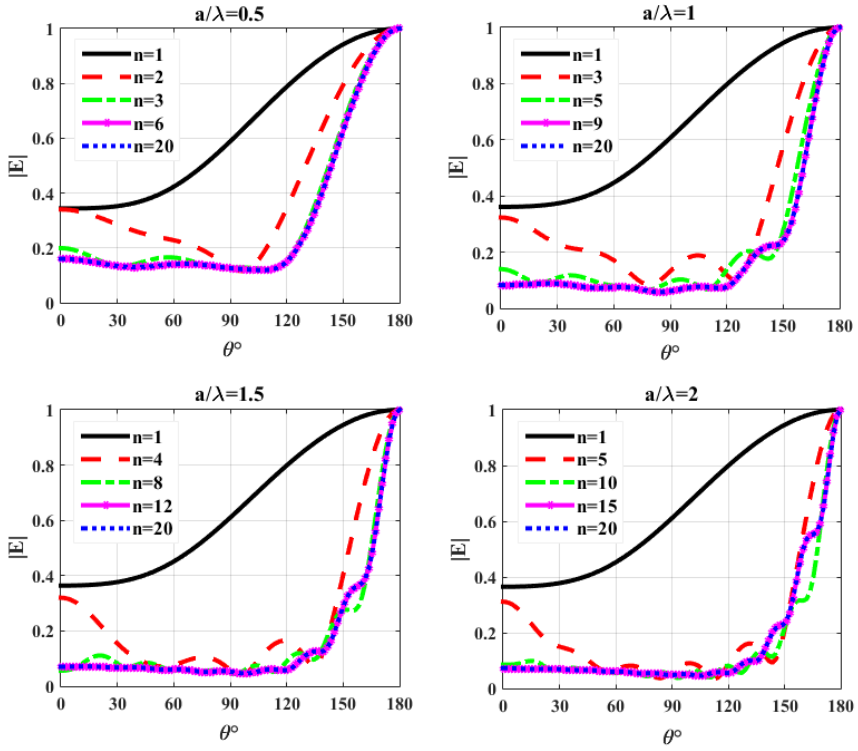

Fig. 4. Convergence study, the normalized absolute value of scattered electric far-field pattern for different number of terms in the summation of (30).

in numerical implementation, this limitation persists [38]. In order to compare our numerical results with those obtained from a commercial software, the sphere with radius equal to $\lambda/3$ for the two limiting cases, PEC and PMC, are simulated using FEKO with its method of moment solver. It is worth mentioning that in this case only the first 5 terms are sufficient for the proposed DGF results to be converged. Moreover, to match the FEKO results to that of DGF, 100 triangular mesh per lambda (more than 33000 meshes) were used and it took more than 30 minutes to run on an *Intel Core i7 8700K CPU, 64 GB RAM* desktop computer while the DGF method took less than 1 second on the same computer. Besides, a memory of 19.5 GB has been allocated for all processes in FEKO. The results are shown in Fig. 7 which are in excellent agreement.

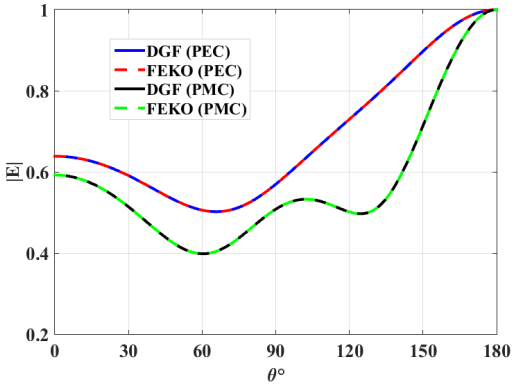

Fig. 7. Comparison of far-field pattern obtained by the DGF method and those of FEKO for PEC and PMC sphere due to a HED.

B. VED

In the case that the radiation source is located vertically with respect to the PEMCS with current moment c pointed in the z-direction and located at $R'=b,\theta'=0,\varphi'=0$, we let

$$\overline{J}(\overline{R'})=c\frac{\delta(R'-b)\delta(\theta'-0)\delta(\varphi'-0)}{b^2\sin\theta'}\hat{z}. \tag{38}$$

Following the same procedure as HED, the scattered field from PEMCS is

$$\overline{E}_s\left(\overline{R}\right)=\frac{k\omega\mu_0 c}{4\pi kb}\sum_{n=1}^{\infty}(2n+1)\\ h_n^{(1)}(kb)\left\{\left(\mathrm{B}^{TM}\right)\overline{N}_{e0n}^{(1)}(k)\right\} \tag{39}$$

Since $\theta'=0$ and $\varphi'=0$, the VED is directed along $\widehat{R}$ and hence only $\overline{N}_{e0n}(k)$ is nonzero. The scattered field in $x-z$ plane is plotted in Fig.8 for the PEMC parameter $\alpha=30°$. In order to calculate scattered electric far-field, again we substitute far-field approximation (32) into (39). The result is

$$E_{s,\theta}\left(\overline{R}\right)=\frac{\omega\mu_0 c}{4\pi b}\sum_{n=1}^{\infty}(2n+1)(-j)^n\frac{e^{jkR}}{kR}\\ h_n^{(1)}(kb)\left\{\left(\mathrm{B}^{TM}\right)\frac{\partial}{\partial\theta}P_n^0(\cos\theta)\right\} \tag{40}$$

Unlike HED, the scattered field for VED, consists only co-polarized component. The co-polarized scattered field as a function of α for $\theta=0$ is plotted in Fig. 9. As before only the first 5 terms are sufficient for the summation in (40) to converge.

This article has been accepted for publication in a future issue of this journal, but has not been fully edited. Content may change prior to final publication. Citation information: DOI 10.1109/TAP.2020.3037726, IEEE Transactions on Antennas and Propagation

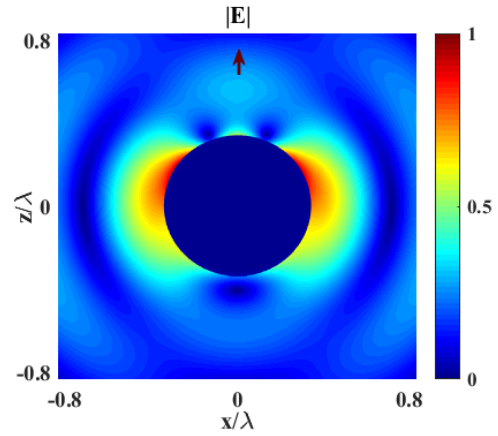

Fig. 8. The normalized absolute value of scattered field in $x-z$ plane due to a z-directed VED for $\alpha = 30°$.

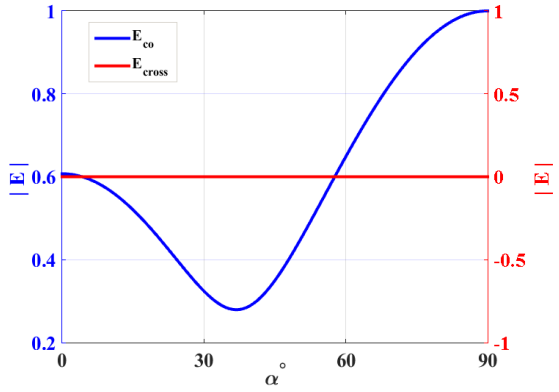

Fig. 9. Co- and cross-polarized terms of normalized absolute value of scattered electric far-field versus $\alpha°$ at $\theta = 0°$ for VED.

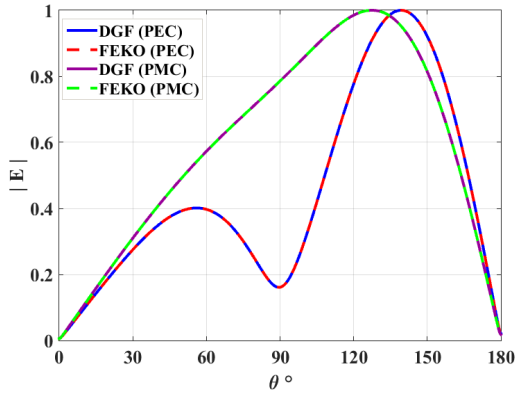

Fig. 10. Comparison of far-field pattern obtained by the DGF method and those of FEKO for PEC and PMC sphere due to a VED.

The VED scattering from the PEMCS with radius equal to $\lambda/3$ is also simulated using FEKO for the two limiting cases, PEC and PMC. The results are compared with those obtained from DGF and plotted in Fig. 10 which are in excellent agreement.

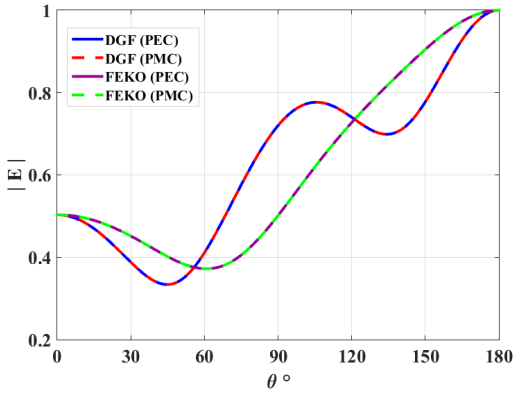

Fig. 11. Comparison of far-field pattern obtained by the DGF method and those of FEKO for PEC and PMC sphere due to plane wave illumination.

C. plane wave

As final example the plane wave scattering from a PEMCS is obtained by moving the HED far away from the sphere. Letting b tend to infinity ($b \to \infty$), the spherical Hankel function can be replaced by its asymptotic form as

$$h_n^{(1)}(kb) \simeq (-j)^{n+1}\frac{e^{jkb}}{kb}, \qquad \frac{\left[kbh_n^{(1)}(kb)\right]'}{kb} \simeq (-j)^n\frac{e^{jkb}}{kb}. \tag{41}$$

By substituting (41) in (30), the scattered field from a PEMCS due to plane wave illumination, is obtained by

$$\overline{E}_s(\overline{R}) = \omega\mu_0 c\frac{e^{jkb}}{4\pi b}\sum_{n=1}^{\infty}\frac{2n+1}{n(n+1)}(-j)^n \left\{\begin{array}{l}\left(-jB^{TE}+B^{TM}\right)\overline{N}_{e1n}^{(1)}(k)+\\ \left(-jA^{TE}+A^{TM}\right)\overline{M}_{o1n}^{(1)}(k)\end{array}\right\}. \tag{42}$$

Again, for calculating far-field scattering one should substitute (32) in (42). The final result reads as

$$E_{s,R} \simeq 0, \tag{43}$$

$$E_{s,\theta} = \omega\mu_0 c\frac{e^{jkb}}{4\pi b}\frac{e^{jkR}}{kR}\sum_{n=1}^{\infty}\frac{2n+1}{n(n+1)}(-1)^n \left\{\begin{array}{l}\left(-jB^{TE}+B^{TM}\right)N_\theta-\\ \left(A^{TE}+jA^{TM}\right)M_\theta\end{array}\right\}, \tag{44}$$

$$E_{s,\varphi} = \omega\mu_0 c\frac{e^{jkb}}{4\pi b}\frac{e^{jkR}}{kR}\sum_{n=1}^{\infty}\frac{2n+1}{n(n+1)}(-1)^n \left\{\begin{array}{l}\left(-jB^{TE}+B^{TM}\right)N_\varphi+\\ \left(A^{TE}+jA^{TM}\right)M_\varphi\end{array}\right\}. \tag{45}$$

In Fig.11 the far-field pattern obtained by the DGF method is compared with those of FEKO. As can be seen the results are in excellent agreement.

IV. Conclusion

In this paper, we have derived the DGF for a PEMCS of an arbitrary radius employing the SSP and the well-known Ohm-Rayleigh method. The derived DGF was used to extract the

scattered field caused by different current sources including HED, VED and plane wave illumination. Numerical results were shown and compared with those obtained by FEKO which were in excellent agreement. Furthermore, the effect of PEMC parameter on the scattered field was investigated. This method is very fast and accurate hence it can be used as an accuracy benchmark for existing full-wave software. The importance of the PEMC boundary lies on the fact that it can produce cross-polarized reflection with respect to the incident wave which may have different applications in microwave and antenna engineering including polarization rotation and co-polarized radar cross section reduction. Extracting DGF for PEMCS coated with dielectric layers is the subject of our future work.

REFERENCES

[1] M. Sadiku, *Numerical techniques in electromagnetics.* New York, NY, USA: CRC Press., 2000.

[2] F. M. Kahnert, "Numerical methods in electromagnetic scattering theory ," *Journal of Quantitative Spectroscopy and Radiative Transfer,* vol. 79, pp.775-824, June 2003.

[3] D. C. Tzarouchis, P. Yl-Oijala, A. Sihvola, "Resonant scattering characteristics of homogeneous dielectric sphere," *IEEE Transactions on Antennas and Propagation,* vol. 65, no. 6, pp.3184-3191, 2017.

[4] R. A. Shore, "Scattering of an Electromagnetic Linearly Polarized Plane Wave by a Multilayered Sphere: Obtaining a computational form of Mie coefficients for the scattered field," *IEEE Transactions on Antennas and Propagation,* vol. 57, no. 6, pp.69-116, 2015.

[5] C. Tai, *Dyadic Green functions in electromagnetic theory,*. 2nd ed., New York, NY, USA: IEEE Press., 1994.

[6] L. W. Li, P. S. Kooi, M. S. Leong, and T. S. Yeo, "Electromagnetic Dyadic Greens Function in Spherically Multilayered Media," *IEEE Transaction on Microwave Theory and Techniques,* vol. 42, no.12, December 1994.

[7] A. Fallahi, and B. Oswald, "On the Computation of Electromagnetic Dyadic Greens Function in Spherically Multilayered Media," *IEEE Transaction on microwave theory and techniques,* vol. 59, no.6, June 2011.

[8] E. L. Tan and S. Y. Tan, "Unbounded and scattered field representations of the dyadic Greens functions for planar stratified bianisotropic media," *IEEE Transactions on Antennas and Propagation,* vol. 49, no.8, pp. 1218-1225, Aug. 2001.

[9] L. W. Li, P. S. Kooi, M. S. Leong, and T. S. Yeo , "Dyadic Greens Functions Inside/Outside a Dielectric Elliptical Cylinder: Theory and Application," *IEEE Transactions on Antennas and Propagation,* vol. 51, no. 3, March 2003.

[10] L. W. Li, M .S. Leong, P. S. Kooi, and T. S. Yeo, "Spheroidal Vector Wave Eigen-function Expansion of Dyadic Greens Functions for a Dielectric Spheroid," *IEEE Transactions on Antennas and Propagation,* vol. 49, no. 4, April 2001.

[11] K. Masumnia-Bisheh, M. Ghaffari-Miab and K. Forooraghi, "Dyadic Greens' function of a conical cavity with impedance spherical cap," *IEEE Transactions on Antennas and Propagation,* vol. 16, no. 11, pp. 6015-6022, 2018.

[12] G. D. Kolezas and G. P. Zouros, "CFVIE formulation for EM scattering on inhomogeneous anisotropicmetallic objects," *IEEE Transactions on Antennas and Propagation,* vol. 65, no. 7, pp. 3788-3793, 2017.

[13] T. Danov and T. Melamed,"Spectral analysis of relativistic dyadic Greens function of a moving dielectric-magnetic medium," *IEEE Transactions on Antennas and Propagation,* vol. 59, no. 8, pp. 2973-2979, Aug. 2011.

[14] F. Mesa, R. Marques, and M. Horno,"A general algorithm for computing the bidimensional spectral Greens dyad in multilayered complex bianisotropic media: The equivalent boundary method," *IEEE Trans. Microw. Theory Tech.,* vol. 39, no. 9, pp. 1640-1649, Sep. 1991.

[15] S. Bassiri, N. Engheta, and C. H. Papas, "Dyadic Greens function and dipole radiation in chiral media," *Alta Freq.,* vol. 55, no. 2, pp. 83-88, 1986.

[16] I. V. Lindell, and A. H. Sihvola, "Perfect electromagnetic conductor," *Journal of Electromagnetic waves and Applications,* vol. 19, no. 7, pp. 861-869, 2005.

[17] I. V. Lindell, and A. H. Sihvola, "Realization of the PEMC boundary," *IEEE Transactions on Antennas and Propagation,* vol. 53, no. 9, pp. 3012-3018, September 2005.

[18] I. V. Lindell, and A. H. Sihvola, "Losses in the PEMC Boundary," *IEEE Transactions on Antennas and Propagation,* vol. 54, no. 9, September 2006.

[19] R. Ruppin, "Scattering of electromagnetic radiation by a perfect electromagnetic conductor sphere," *J. Electromagn. Waves Appl.,* pp. 1569-1576, 2006.

[20] R. Ruppin, "Scattering of electromagnetic radiation by a perfect electromagnetic conductor cylinder," *J. Electromagn. Waves Appl.,* pp. 1853-1860, 2006.

[21] S. Ahmed, Q.A. Naqvi, "Electromagnetic scattering from a perfect electromagnetic conductor cylinder buried in a dielectric half space," *Progress In Electromagnetics Research,* vol. 78, pp. 25-38, 2008.

[22] S. Ahmed, Q.A. Naqvi, "Electromagnetic scattering from parallel perfect electromagnetic conductor cylinder of circular cross-section using an iterative procedure," *Journal of Electromagn. Waves Appl.,* vol. 22, no. 7, pp. 987-1003, 2008.

[23] K. Hamid, F.R. Cooray, "Scattering by a perfec electromagnetic conductiong elliptic cylinder," *Progress In Electromagnetics Research Letters,* vol. 10, pp. 59-67, 2009.

[24] A. Ghaffar,S.I. Ahmad, R. Fazal , S. Shukrullah, Q. A. Naqvi, "Scattering of electromagnetic wave by perfect electromagnetic conductor (PEMC) sphere placed in chiral media ," *Optik,* vol. 21, pp. 4947-4951, 2013.

[25] V. Nayyeri, M. Soleimani, M. Dehmollaian, and J. Rashed-Mohassel, "Reflection from Stratified Media Backed by a Perfect Electromagnetic Conductor (PEMC)," *IEEE Transactions on Antennas and Propagation,* vol.60, no. 10, 2012.

[26] M. A. Fiaz, "Investigating the reduction of cross-polarized Gaussian beam scattering from a PEMC buried cylinder coated with a topological insulator," *Applied optics,* vol.57, no. 27, pp. 7830-7836, 2018.

[27] I. V. Lindell, and A. H. Sihvola,"Electromagnetic boundary and its realization with anisotropic metamaterial," *Phys. Rev. E.* vol. 79, no. 2, 2009.

[28] A. Shahvarpour, T. Kodera, A. Parsa, and C. Caloz, "Arbitrary electromagnetic conductor boundaries using Faraday rotation in a grounded ferrite slab," *IEEE Trans. Microw. Theory Tech.,* vol. 58, no. 11, pp. 2781-2793, 2010.

[29] D. L. Sounas and C. Caloz, "Electromagnetic nonreciprocity and gyrotropy of graphene," *App. Phys. Lett.,* vol. 98, no. 2, 2011.

[30] C. Caloz, "Next-generation metamaterials for unprecedented microwave systems," *in Proc. 10th Int. Conf. on Telecommunication in Modern Satellite Cable and Broadcasting Services (TELSIKS),* pp. 3-12, 2011.

[31] M. Rasouli Disfani, K. Vafi, M. S. Abrishamian, "Dyadic Greens function of a PEMC cylinder," *Applied Physics A,* pp. 765-769, 2011.

[32] J. Komijani, J. Rashed-Mohassel, "Symmetrical properties of dyadic Greens functions for mixed boundary conditions and integral representations of the electric fields for problems involving a PEMC," *IEEE Transactions on Antennas and Propagation,* vol. 57, no. 10, pp.3199-3204, 2009.

[33] N. Moghadasi, R. A. Sadeghzadeh, R. HafeziFard, "Dyadic Green's function for a dielectric layer on a PEMC elliptical cylinder," *IEICE Electronics Express,* vol. 7, no. 14, pp. 1034-1043, 2010.

[34] J. Komijani, J. Rashed-Mohassel, "Dyadic Green Functions for a Dielectric Layer on a PEMC Plane," *Progress In Electromagnetics Research,* vol. 6, pp. 9-22, 2009.

[35] R. Ruppin, "Scattering of electromagnetic radiation by a coated perfect electromagnetic conductor sphere," *Progress In Electromagnetics Research,* vol. 8, pp. 53-62, 2009.

[36] I. V. Lindell, and A. H. Sihvola, "Transformation Method for Problems Involving Perfect Electromagnetic Conductor (PEMC) Structures," *IEEE Transactions on Antennas and Propagation,* vol. 53, no. 9, September 2005.

[37] V. Nayyeri, M. Soleimani, and M. Dehmollaian, "Modeling of the perfect eletromagnetic conducting boundary in the finite difference time domain method," *Journal of Radio Science,* vol. 48, 2013.

[38] R. Miri, M. Ghaffari-Miab, "Finit difference generated transient potentials of open-layered media by parallel computing using openMP, MPI, openACC and CUDA," *IEEE Transactions on Antennas and Propagation,* vol. 67, no. 10, 2019.